Journal of Geochemical Exploration 221 (2021) 106679

Contents lists available at ScienceDirect

Journal of Geochemical Exploration

journal homepage: www.elsevier.com/locate/gexplo

Tracking hydrothermal events using zircon REE geochemistry from the Carajás Mineral Province, Brazil

Maurício L. Borba [a,*], Colombo C.G. Tassinari [a], Fernando M.V. Matos [b], Kei Sato [a], Sergio Huhn [b], Samuel N. Ferreira [b], Carlos A. Medeiros [b]

[a] Institute of Geosciences, University of São Paulo, São Paulo 05508-080, Brazil
[b] VALE, Santa Luzia, MG 34730-010, Brazil

ARTICLE INFO

Keywords:
Hydrothermal zircon
U-Pb SHRIMP
REE in zircon
Carajás
IOCG

ABSTRACT

Zircon geochemistry and geochronology are powerful tools in the study of multistage cratonic settings, yielding information on ages and distinguishing terranes. The Carajás Mineral Province (CMP) SE of the Amazonian Craton is renowned for its complex tectonic evolution and notable mineral deposits endowment, such as the giant iron-oxide-copper-gold (IOCG)-type Sossego and Salobo. Tectonic, magmatic, metamorphic, and hydrothermal event sequences imprint their records regionally and deposit scales that, in most cases, are difficult to identify. Basement and wall-rock samples from the southern portion of the CMP's, Sossego area were selected and analyzed using sensitive high-resolution ion microprobe (SHRIMP). Cathodoluminescence images guided the morphological and textural characterization and spot location. U-Pb and rare earth elements (REE) analyses using SHRIMP provided ages and trace element contents leading to classification of zircon type as magmatic, hydrothermally altered magmatic, or hydrothermal zircon. Hydrothermal zircon is characterized by anomalous morphology and REE and U contents, and these features have prompted the identification of an Archean hydrothermal event in the province. These zircon classifications indicate a circa 2.54 Ga hydrothermal event in the southern region of Carajás, likely associated with main shear zone movements (Carajás Fault). The 2.54 Ga event is well constrained to the Carajás northern zone and has not been indicated in the southern region. The magmatic and hydrothermally altered zircons indicate ages around 2.95 Ga and 2.74 Ga, coinciding with the zone's known ages, with better resolution achieved using SHRIMP. The use of zircon type classification in cratonic terranes to track hydrothermal events offers original possibilities and represents new frontiers in mineral exploration.

1. Introduction

Zircon is an accessory mineral that has been widely used for several decades in U-Pb dating. More recently, its rare earth elements (REE) content has gained traction as a tool in provenance determination, hydrothermal evaluation, and estimation of magma and melt signatures (Ballard et al., 2002; Fu et al., 2009; Hanchar and Van Westrenen, 2007; Hoskin, 2005; Zhong et al., 2018). The hydrothermal effect or genesis of zircon has been described with respect to different geological environments, from cratonic terranes (Claoué-Long et al., 1990; Corfu and Davis, 1991; Hoskin, 2005) to porphyry and volcanic-hosted massive sulfide (VHMS) deposits (Loader et al., 2017; Toscano et al., 2014). However, no consensus has yet been reached with regard to how hydrothermal fluids act on zircon lattice and trace element behavior, although studies have indicated geochemical differences compared to magmatic zircons (Lawrie et al., 2007; Rubin et al., 1989; Toscano et al., 2014; Zhong et al., 2018). Most findings highlight hydrothermal zircon's anomalous Eu and Ce contents and enrichment in other light rare earth elements (LREE), such as La and Pr, compared to magmatic zircon (Ballard et al., 2002; Smythe and Brenan, 2016 and references therein); however, in most cases, the La contents lie under the equipment's detection limit.

The Carajás Mineral Province (CMP) (Vasquez et al., 2008) lies within the Amazonian Craton (Santos et al., 2000; Tassinari and Macambira, 1999) in northern Brazil and is well endowed with several mineral deposits, including the giant Salobo and Sossego iron-oxide-copper-gold (IOCG) deposits (Bettencourt et al., 2015; Grainger et al., 2008; Monteiro et al., 2008; Xavier et al., 2012 and references therein). Several authors (Feio et al., 2013; Machado et al., 1991; Moreto et al., 2015b; Sardinha et al., 2006; Tallarico et al., 2004; Tassinari et al.,

* Corresponding author.
E-mail address: mauriciolborba@usp.br (M.L. Borba).

https://doi.org/10.1016/j.gexplo.2020.106679
Received 12 May 2020; Received in revised form 20 September 2020; Accepted 27 October 2020
Available online 29 October 2020

2003) have presented geochronological data for regional rocks and ore deposits. These findings indicate Archean and Paleoproterozoic ages for rocks and ore, locating mineralization events at circa 2.7 Ga, 2.5 Ga, and 1.88 Ga, coincident with magmatism, and most deposits indicate more than one period with respect to ore bearing.

A hydrothermal event around 2.2–2.3 Ga, so far unrelated to magmatism, has been proposed for the province (Borba et al., 2019), and these ages were registered at the Sossego deposit, the Corta Goela prospect, and in basement rocks (Borba et al., 2019; Marschik et al., 2003; Moreto et al., 2015a; Pollard et al., 2018; Tavares, 2015). These occurrences each exhibit a close relationship with the regional structure of the Carajás Fault (Pinheiro et al., 1997) and may represent evidence of structural movement. Alkaline magmatism occurred at 1.88 Ga (Machado et al., 1991) throughout the province, and some IOCG deposits mineralizations are coeval with this magmatism (Grainger et al., 2008; Moreto et al., 2015b; Tallarico et al., 2005; Xavier et al., 2012, among others).

This study aims to date the hydrothermally altered basement and wall-rocks and to analyze the influence of hydrothermal processes on REE in zircon. To comprehend and identify the REE patterns and to use them as a tool for mineral exploration, three types of zircon were distinguished: magmatic, hydrothermally altered magmatic, and hydrothermal. We present cathodoluminescence images of zircon grains combined with the U-Pb dates of six granitoids with different hydrothermal alterations. The REE and U contents are used to determine zircon type. Terranes with superimposed tectonic cycles and successive

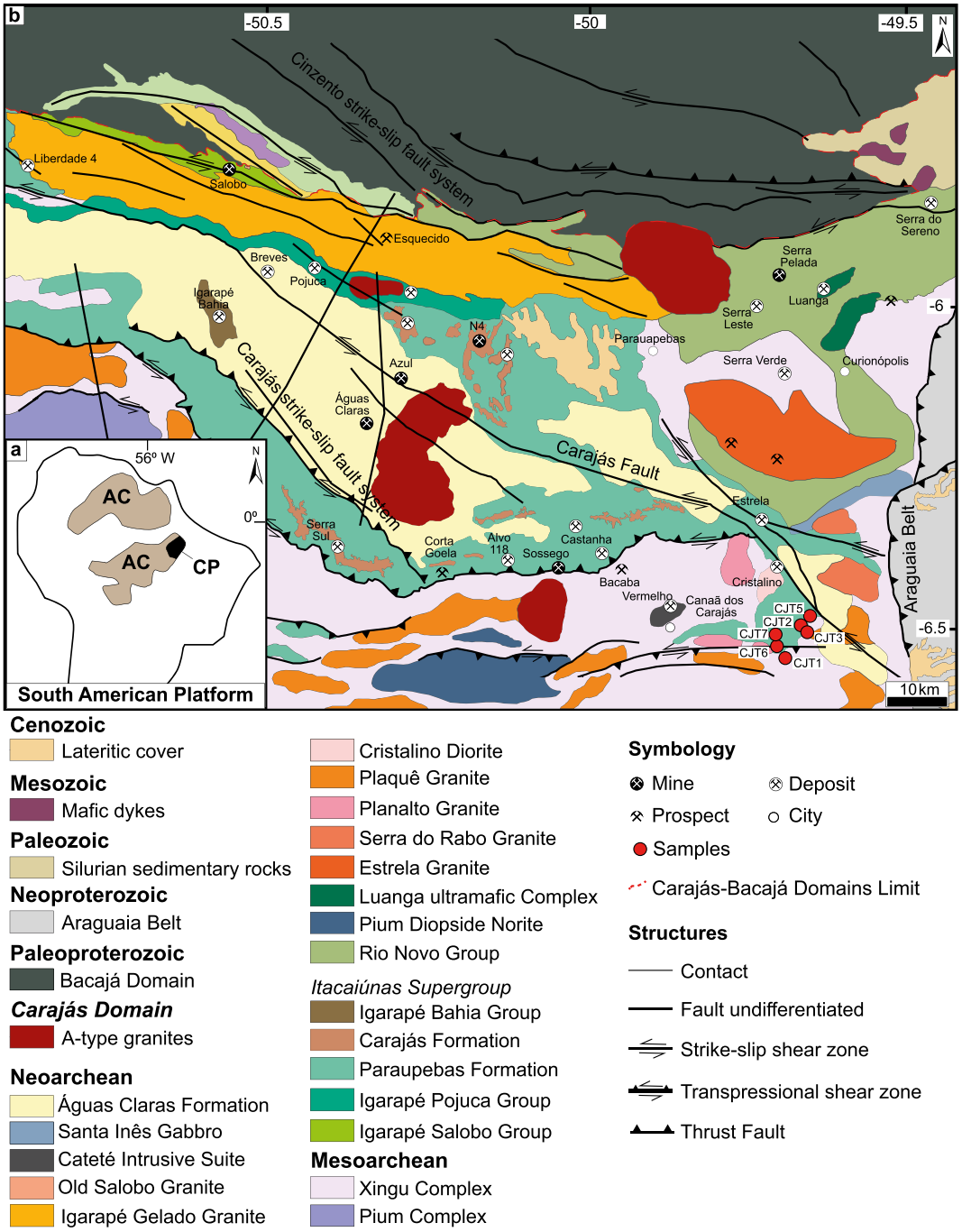

Fig. 1. Geological map of the study area. a) Location in the South American Platform, AC = Amazonian Craton; CP = Carajás Province. b) Geological map of Carajás Province and samples location (Vasquez et al., 2008).

hydrothermal occurrences are challenging for geological surveys, and hydrothermal zircon geochemistry has significant potential as a proxy for mineral exploration.

2. Geological setting

The Amazonian Craton is composed of two shields, Guyana to the north and Central Brazil to the south, separated by the Paleozoic Solimões-Amazonas Sedimentary Basin. The CMP lies in the southeast of the craton and is divided into two tectonic domains, the Neoarchean Carajás (Fig. 1) to the north and the Mesoarchean Rio Maria to the south (Santos, 2003). To the north, the province is limited by the Bacajá Domain, with Proterozoic to Cenozoic sequences of the Amazon Basin, with the Cinzento Shear Zone marking the contact (Pinheiro et al., 1997). The eastern border of the province is formed by the Neoproterozoic Araguaia Belt, while to the west lie the Paleoproterozoic plutonic and volcanic sequences with the Santana do Araguaia Domain to the south (Tassinari and Macambira, 1999). The Rio Maria Domain is composed primarily of greenstone belt associations, mafic-ultramafic rocks, and granites of Mesoarchean age (Almeida et al., 2010; Dall'Agnol et al., 2005; Macambira et al., 2009; Oliveira et al., 2009). The Carajás Domain basement comprises the mafic granulites of the Pium Complex (Vasquez et al., 2008) and various rocks from the Xingu Complex (Pidgeon et al., 2000; Almeida et al., 2011; Feio et al., 2013; Moreto et al., 2015a and references therein) with ages around 2.95 to 3.0 Ga.

The Itacaiúnas Supergroup, in the central portion of the province, is a 2.76- to 2.74-Ga sequence that forms part of the Neoarchean Carajás Basin and is composed primarily of bimodal metavolcanics, metasedimentary rocks, and banded iron formations (DOCEGEO, 1988; Machado et al., 1991; Trendall et al., 1998; Tallarico et al., 2005). Upwards in the stratigraphy the Rio Novo Group (Hirata et al., 1982) is composed of tholeiitic metavolcanics, gabbro, schists, and meta-graywacke. The ultramafic layered intrusions, the Luanga and Cateté Intrusive Suites, intrude into the Rio Novo Group at 2.76 Ga (Machado et al., 1991; Teixeira et al., 2015 and references therein). A prominent 2.76- to 2.57-Ga succession of granitic plutons (Machado et al., 1991; Sardinha et al., 2006; Feio and Dall'Agnol, 2012; Feio et al., 2013; Moreto et al., 2015b) occurs in the area (e.g. Estrela, Serra do Rabo, Planalto, Plaquê, Bom Jesus, Cristalino, Igarapé Gelado, among others). These units are covered by the Águas Claras Formation sedimentary sequences (Vasquez et al., 2008).

Paleoproterozoic alkaline granites with ages around 1.88 Ga. (Machado et al., 1991) were emplaced during the extensive tectonic regime. Certain granites are considered to contribute to mineralizations, such as Breves (Tallarico et al., 2004), Gameleira (Machado et al., 1991; Marschik et al., 2005) and Estrela (Lindenmayer et al., 2005). This granitogenesis also contributed directly to Sossego and 118 Paleoproterozoic mineralization deposits (Grainger et al., 2008; Moreto et al., 2015b and references therein).

Another hydrothermal episode circa 2.2–2.3 Ga without magmatic relation in the province has been posited (Borba et al., 2019), based primarily on ^{40}Ar-^{39}Ar geochronology. Ages obtained from hornblende and biotite from the Sossego deposit, Corta Goela prospect, and basement rocks (Borba et al., 2019; Marschik et al., 2003; Pollard et al., 2018; Tavares, 2015) and U-Pb in monazite at Sossego (Moreto et al., 2015b) indicate this Rhyacian hydrothermal event. The existence of magmatism at this time is unknown in the southern region of the CMP. However, samples from these ages are closely related to the regional structure of the Carajás Fault (Pinheiro et al., 1997) and may be a record of these structures' movements. Although some researchers considered that this Rhyacian age may be a reflex of the 1.88 Ga magmatism that produced recirculation of hydrothermal fluids affecting the isotopic system (Moreto et al., 2015b; Pollard et al., 2018), other studies have argued that this is an isolated event (Borba et al., 2019; Marschik et al., 2003; Tavares, 2015) that is structurally controlled. Notably, the CMP presents a succession of igneous intrusions and extensional events of transpressive and transtensional character (Pinheiro et al., 1997; Holdsworth and Pinheiro, 2000), demonstrating a complex tectonic evolution from Archean to Paleoproterozoic.

3. Sampling and analytical procedures

Multiple outcrop basement and deposit wall-rock samples (Table 1) were collected for U-Pb and REE in zircon using sensitive high-resolution ion microprobe (SHRIMP). This study was carried out on the VALE samples collection, and these rocks are related to the main structure associated with the IOCG deposits. Complete petrography and thin section descriptions were developed at the mining company's request (VALE, 2015), before these isotopes studies. Selected samples were crushed (~2 kg) and sieved, and the zircon grains were concentrated using an isodynamic magnetic separator and heavy liquids (methylene iodide). The zircon concentrate was handpicked, and 80–100 crystals were mounted on a double-sided adhesive plate along with the standards (TEMORA 2 and NIST 610). Subsequently, epoxy resin was added and dried, and the mount was polished to reveal the zircons surfaces.

Scanning electron microscope and cathodoluminescence (SEM-CL) imaging using a Quanta 250 FEI with XMAX CL detector (as per Sato et al., 2014) at the Geochronological Research Center at the University of São Paulo exposed the zircon's internal complexities.

The analyses were conducted using the SHRIMP-IIe at the High-Resolution Geochronology Laboratory at the University of São Paulo, and the equipment conditions and procedures were similar to those described by Williams (1998). Suitable zircon crystals from each sample were analyzed, avoiding where possible fractured and/or metamitic grains and microinclusion areas (e.g., apatite). Data acquisition was performed with six mass range scans for zircon with one standard for every four zircons. Age calculations required adjustments for common Pb using the measured ^{204}Pb and the relevant common Pb compositions from Stacey and Kramers' (1975) model. For data evaluation and ages, SQUID-2.5 (Ludwig, 2009) and ISOPLOT3 (Ludwig, 2003) were used (complete procedures are described in Sato et al. (2014)).

To measure the zircon's REE isotopic composition, the spots were placed near the U-Pb spot. The elements analyzed were Zr, La, Ce, Pr, Nd, Sm, Eu, Gd, Tb, Dy, Ho, Er, Tm, Yb, and Lu. Data were obtained as masses and then reduced into CI-chondrite-normalized (McDonough and Sun, 1995) elements. The complete procedure and equipment setting are described in Sato et al. (2016), and the detection limits for SIMS are accordance with Wiedenbeck et al. (2004).

4. Results

The sample descriptions indicate that CJT1 is a deformed tonalite of porphyritic texture and foliated matrix comprising quartz and

Table 1
Summary of selected samples and its classification and related hydrothermal minerals.

Sample Id	Geological context	Lithology	Hydrothermal minerals
CJT1	Campina Verde Tonalite	Tonalite	Fluorite, scapolite, albite, magnetite
CJT2	Umuarama Granite	Monzogranite	Biotite, magnetite, amphibole, fluorite, chlorite, apatite
CJT3	Umuarama Granite	Pegmatite	Tourmaline, biotite
CJT5	Canaã dos Carajás Granite	Monzogranite	Scapolite, fluorite, apatite, calcite
CJT6	Planalto Granite Suite	Monzogranite	Biotite
CJT7	Bom Jesus Granite	Monzogranite	Albite, scapolite, fluorite

plagioclase, with oriented biotite (5–8%). The rock presents plagioclase and quartz veinlets. Discrete hydrothermal alteration is observed, marked by silicification and chloritization. Sample CJT2 is a foliated monzogranite with phaneritic texture, composed of quartz, k-feldspar, plagioclase, biotite, and amphibole. Sample CJT3 is a pegmatite vein associated with the CJT2 monzogranite, presenting a porphyritic texture, and composed of quartz, k-feldspar, and biotite with sparse amphibole. Sample CJT5 is a foliated monzogranite, with phaneritic texture, composed of quartz, k-feldspar, plagioclase, biotite, and amphibole. CJT5 presents slight hydrothermal alteration, structurally oriented, marked by silicification and sparse fluorite. Sample CJT6 is a foliated monzogranite, with phaneritic texture, and a quartz, k-feldspar, plagioclase, and biotite mineral assembly. This sample shows slight hydrothermal alteration with amphibole, chlorite, and chalcopyrite. Sample CJT7 is a monzogranite with phaneritic texture, formed by quartz, k-feldspar, plagioclase, biotite, and muscovite, hydrothermal fluorite, and scapolite. The main hydrothermal minerals are indicated in the Table 1 and were consulted on VALE (2015).

SEM-CL images indicate variations in zircon morphology, internal zonation and hydrothermal alteration grade according to the sample (Fig. 2). The Campina Verde Tonalite (CJT1) grains are euhedral and fractureless, and most crystals are not metamictized, with inherited cores in some cases and sizes ranging from 200 to 400 μm (Fig. 2A). These crystals have oscillatory zonation, with diffuse gray borders, suggesting moderate hydrothermal alteration (Fig. 2B). Umuarama Granite (CJT2) zircons are subhedral and range from 100 to 200 μm. They are typically dark gray, and devoid of oscillatory zonation. Several crystals showed metamictization and microinclusions and were divided into two groups: light gray with massive appearance and dark gray to black with spongy texture (Fig. 2A). Additionally, the Umuarama Pegmatite (CJT3) presents the same type of zircon as the associated sample previously described (Fig. 2A). The Canaã dos Carajás Granite (CJT5) zircons are subhedral and range from 50 to 400 μm in length. These crystals can be subdivided into two types: the first comprises light gray crystals with oscillatory zoning, few fractures, and diffuse borders; the second type is dark gray with spongy texture, suggesting hydrothermal alteration (Fig. 2A).

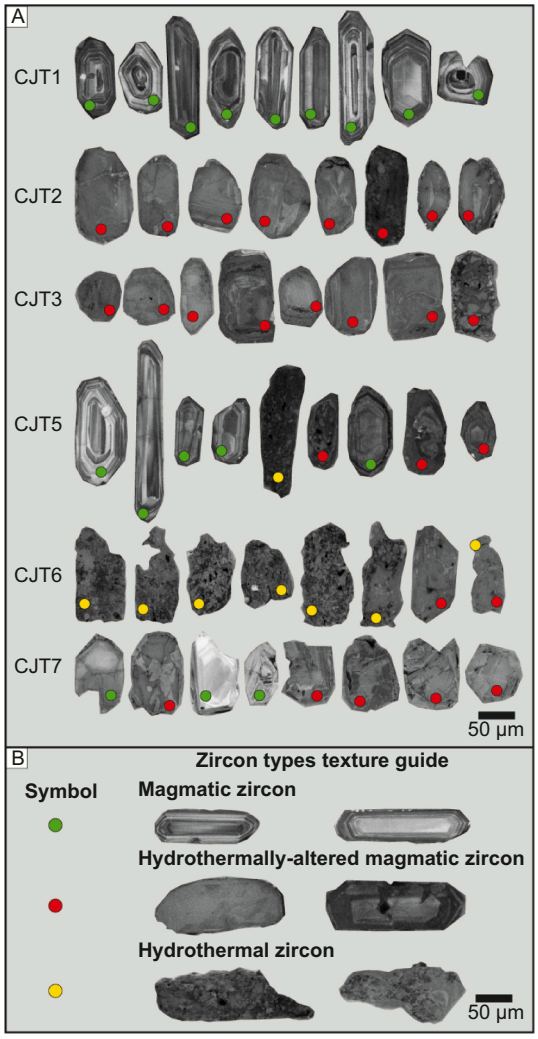

Fig. 2. SEM-Cathodoluminescence images of zircon with discrimination of proposed types of grains. (A) SEM-CL images of selected zircon grains from studied samples. The spot is tagged to identify the zircon type according to the proposed classification (B). (B) Proposed zircon type classification guide according to morphology and textures (color-coded symbols corresponding to zircon type). (For interpretation of the references to color in this figure legend, the reader is referred to the web version of this article.)

Planalto Granite (CJT6) zircon crystals also occur in two types (Fig. 2A), and the first type is subhedral and ranges from 150 to 250 μm in length, has remnant oscillatory zoning, light gray colors, and partial metamictization. This grain type was found in only two crystals in the sample. The second type was the dominant population in the sample, and consisted of zircons that were dark gray, ranging from 80 to 150 μm in length, with diffuse borders and spongy texture (here called "bread-crust" texture). This is considered to be hydrothermal zircon (Fig. 2B).

The Bom Jesus Granite (CJT7) zircons are subhedral, ranging from 150 to 250 μm in length, are light gray in color, and have some inherited cores and oscillatory zoning remnants. Several crystals have diffuse rims and spongy texture, indicating at least partial hydrothermal alteration (Fig. 2A).

The SEM-CL images made it possible to define the crystals' morphology and internal textures and to distinguish at least three types of zircon prior to the SHRIMP analyses: (i) magmatic; (ii) hydrothermally altered and (iii) hydrothermal (Fig. 2B).

4.1. SHRIMP II U-Pb zircon ages

Fig. 3 provides a summary of U-Pb SHRIMP ages diagrams, and the tables of analytical data are included in the Supplementary Material 1.

Sample CJT5 is the Canaã dos Carajás Granite, of which sixteen spots were analyzed. The U content ranges from 95 to 345 ppm, and the $^{232}Th/^{238}U$ ratio is 0.49–169. The analyses indicate a $^{206}Pb/^{238}U$ versus $^{207}Pb/^{235}U$ upper intercept age (Fig. 3D) of 2943 ± 9 Ma (mean square weighted deviation, MSWD = 1.7) and lower intercept at 891 ± 76 Ma.

Thirteen spots were analyzed from the Campina Verde Tonalite (CJT1). The U content ranges from 116 to 518 ppm and the $^{232}Th/^{238}U$ ratios are between 0.23 and 0.69. The analyses indicate a $^{206}Pb/^{238}U$ versus $^{207}Pb/^{235}U$ upper intercept age of 2938 ± 18 Ma (MSWD = 5.7) (Fig. 3A) and lower intercept at 501 ± 150 Ma. While discordant zircons excluded a concordia age (Fig. 3A′), 2938 ± 4.4 Ma (MSWD = 1.8) is interpreted as the magmatic crystallization age.

Sixteen spots were analyzed from the Umuarama Granite sample (CJT2) and the U content ranged from 459 to 949 ppm and the $^{232}Th/^{238}U$ ratio is 0.40–0.89. The ^{204}Pb corrected $^{206}Pb/^{207}Pb$ individual ages, indicating discordances among the crystals in response to Pb loss; however, a $^{206}Pb/^{238}U$ versus $^{207}Pb/^{235}U$ concordia age (Fig. 3B) of 2744 ± 32 Ma (MSWD = 14) provided the crystallization age for the Umuarama Granite. Fourteen spots of the spatially associated Umuarama Pegmatite (CJT3) were analyzed, and the U content ranged from 577 to 1192 ppm and the $^{232}Th/^{238}U$ ratio was 0.19–0.90. The analyses indicate a $^{206}Pb/^{238}U$ versus $^{207}Pb/^{235}U$ upper intercept age (Fig. 3C) of 2732 ± 22 Ma (MSWD = 7.7) and lower intercept at 474 ± 44 Ma.

The Planalto Granite sample (CJT6) presented strongly variable U content (U = 134–2849 ppm), so this sample was analyzed in two rounds. The first attempt considered all crystals while the second

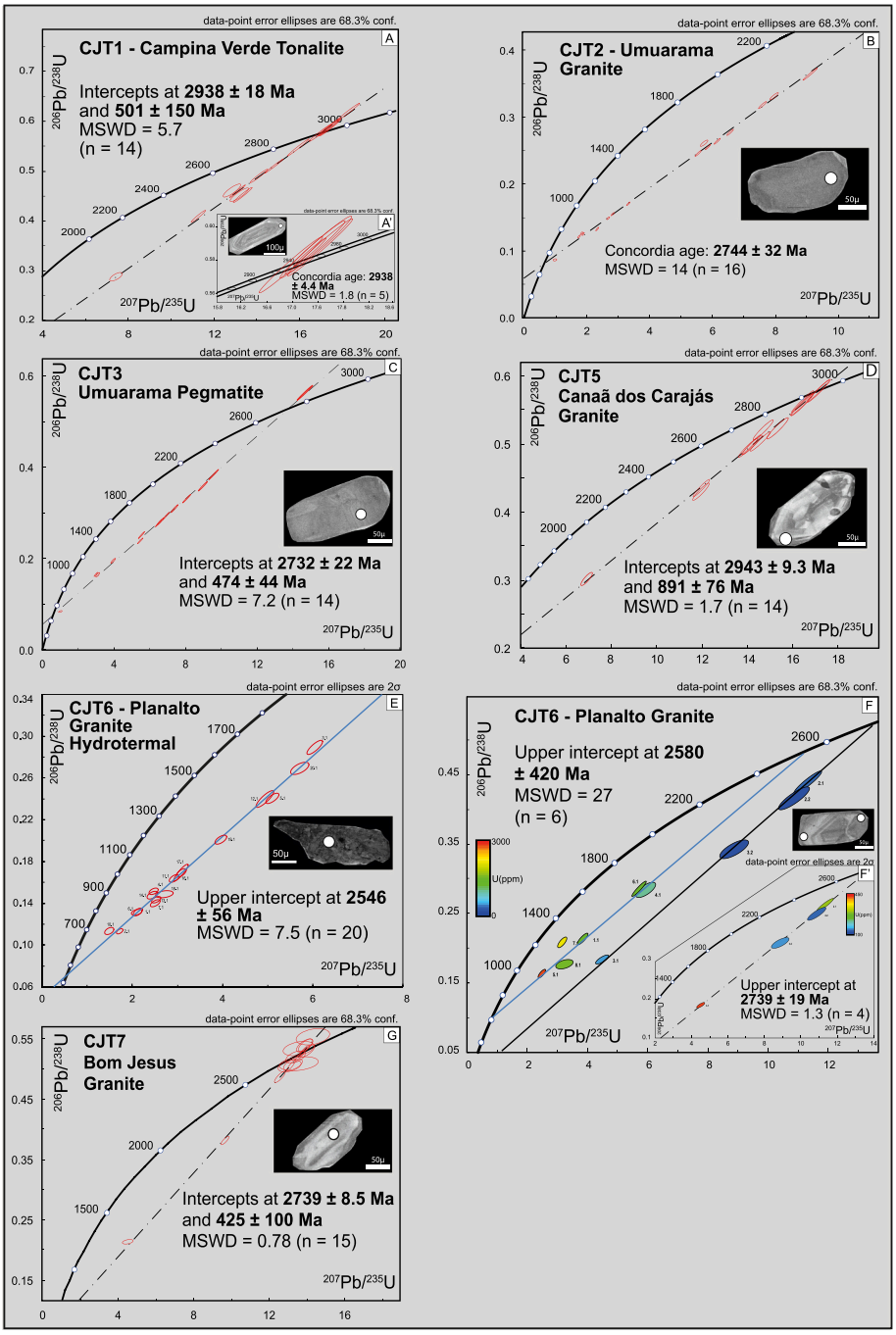

Fig. 3. $^{206}Pb/^{238}U$ vs. $^{207}Pb/^{235}U$ diagrams of zircon—SHRIMP analyses of the studied samples. (A) and (A') CJT1 – Campina Verde Tonalite; (B) CJT2 – Umuarama Granite; (C) CJT3 – Umuarama Pegmatite; (D) CJT5 – Canaã dos Carajás Granite; (E) CJT6 – Planalto Granite – hydrothermal ages; (F) CJT6 – Planalto Granite with indication of U contents; (F') CJT6 – Planalto Granite – magmatic ages; (G) CJT7 – Bom Jesus Granite – magmatic ages.

considered only the hydrothermal crystals. Among the analyzed crystals, only two zircon grains presented regular oscillatory zoning and suitable U and Th contents, in relation to the magmatic samples (Hoskin and Schaltegger, 2003). These selected grains (2.1, 2.2, 3.1, and 3.2, Fig. 3F) are prismatic and euhedral, with crystal lengths ranging from 200 to 250 μm and U content ranging from 134 to 445 ppm, with a $^{232}Th/^{238}U$ ratio of 0.17–0.63. To better illustrate the uranium content, a color scale was used to designate this variation. Once all results are plotted in the diagram, the $^{206}Pb/^{238}U$ versus $^{207}Pb/^{235}U$ upper intercept age is 2580 ± 420 (MSWD = 27) (Fig. 3F), but if only the four selected spots from the zircon with lower U contents are plotted, the $^{206}Pb/^{238}U$ versus $^{207}Pb/^{235}U$ upper intercept age is 2739 ± 19 Ma (MSWD = 1.13) (Fig. 3F′), considered to be the crystallization age of the Planalto Granite. The second round of analyses for the sample CJT6 was conducted on the hydrothermal zircon population. Twenty analytical spots were conducted, and the $^{206}Pb/^{238}U$ versus $^{207}Pb/^{235}U$ upper intercept age was 2546 ± 56 (MSWD = 7.5) (Fig. 3E) with U content varying from 869 to 2359 ppm. The age of 2.54 Ga is considered to be the timing of the hydrothermal alteration.

Fifteen Bom Jesus Granite (CJT7) zircons were analyzed, and the U content was found to range from 49 to 163 ppm, with the exception of one grain that had 678 ppm (metamict crystal, spot 9.1), and the $^{232}Th/^{238}U$ ratio was 0.44–1.33. The analyses indicate a $^{206}Pb/^{238}U$ versus $^{207}Pb/^{235}U$ upper intercept age of 2739 ± 8.5 Ma (MSWD = 0.78)

and lower intercept at 425 ± 100 Ma (Fig. 3G).

4.2. Rare earth elements geochemistry

The CI-chondrite-normalized (McDonough and Sun, 1995) and total REE contents of the zircon samples are indicated in the Supplementary Material 2. REE data were used to classify the zircon as magmatic, hydrothermally altered magmatic, or hydrothermal.

The REE contents of magmatic zircons ranged from 95 to 490 ppm (average 204 ppm, σ = 105.38), and the total LREE contents ranged from 6 to 41 ppm (average 21 ppm, σ = 13.62); for the hydrothermally altered grains, the total REE contents ranged from 128 to 1517 ppm (average 565 ppm, σ = 361.04) and the total LREE contents ranged from 4 to 1139 ppm (average 162 ppm, σ = 241.01); the hydrothermal zircons have total REE contents ranging from 274 to 640 ppm (average 379 ppm, σ = 122.01) and LREE contents vary from 22 to 237 ppm (average 73 ppm, σ = 64.34). Eu/Eu* (Eu anomaly amplitude), where Eu_N = concentration of Eu CI chondrite-normalized, represented by subscript "N" (McDonough and Sun, 1995), and Eu* = $(Sm_N \cdot Gd_N)^{1/2}$ are also indicated for the three zircon types. The magmatic zircon type has Eu/Eu* ranging from 0.19 to 5.09; the hydrothermally altered crystals have values from 0.10 to 4.35; and the hydrothermal crystals range from 0.59 to 3.8.

The analyzed zircons have prominent REE concentrations, particularly for LREE, as La, Ce, and Pr. The La content ranges from 0.027 to 82.99 ppm when all zircon crystals are considered regardless of type. The La ranges from 0.027 to 1.47 ppm in the magmatic zircon and from 0.034 to 82.99 ppm (with an isolated value of 428 ppm) in the hydrothermally altered zircons. Hydrothermal zircon has a La content that ranges from 0.69 to 50.7 ppm, and La is usually below the detection limit for zircon (Hoskin, 2005; Hoskin and Schaltegger, 2003). Ce, Pr, Nd, and Sm also present higher contents than are found in magmatic types as a result of hydrothermal alteration. Samples of the indicated zircons were selected to build the REE versus CI-chondrite diagram (McDonough and Sun, 1995), and the REE patterns are distinguished according to type (Fig. 4). The hydrothermal type is enriched with LREE and does not present the Eu anomaly, showing flattened curves and high REE values.

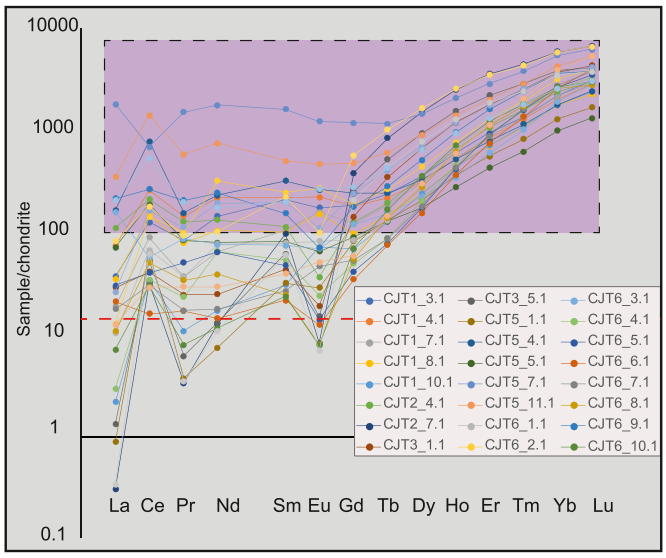

Fig. 4. CI-Chondrite-normalized REE patterns of selected zircon types. The red dashed line separates magmatic zircon from hydrothermally altered zircon, and the light purple area indicates the hydrothermal zircon geochemical signature for these elements. The most prominent differences among these zircon types are in the LREE enrichment rather than in the other REE. (For interpretation of the references to color in this figure legend, the reader is referred to the web version of this article.)

The SEM-CL images combined with the La and U contents and Eu/Eu* and U/Th ratios (Fig. 5) illustrate the differences among zircon types. Magmatic zircons (Fig. 5A, D, E, and E′) show oscillatory zoning; the U contents range from 112 to 435 ppm; Th/U ranges from 0.17 to 1.27; La contents (0.21–051 ppm) are low; and Eu/Eu* is higher than in the other types. Zircon from Figs. E and E′ were not analyzed for REE, because these were from the first attempt for sample CJT6. Hydrothermally altered crystals (Fig. 5A′, B, B′, C, C′, D′, I, and I′) are subhedral with massive texture and higher U contents than the previous type. These zircons have a U-content range of 282 to 995 ppm, while their La contents range from 0.07 to 26.19 ppm. The hydrothermal zircon type (Fig. 5F, F′, G, H, and H′) presents anhedral morphology and "bread-crust" texture, distinct from the other types. The U contents of hydrothermal zircons range from 993 to 1477 ppm and the La content ranges from 0.63 to 7.09 ppm.

5. Discussion

5.1. Ages of intrusions and hydrothermal events

U-Pb ages and REE contents of zircon samples from the southeastern region of the CMP were carried out to track hydrothermal alteration and evaluate its influence on zircon U-Pb ages and trace element behavior.

The U-Pb zircon ages of Canaã dos Carajás Granite and Campina Verde Tonalite are 2943 ± 9.3 Ma (MSWD = 1.7, n = 14) and 2938 ± 4.4 Ma (MSWD = 1.8, n = 5), respectively. These ages are more closely related to those obtained for the Bacaba Tonalite (Moreto et al., 2011), Sequeirinho Granite, and Pista metavolcanic rock (Moreto et al., 2015a, 2015b). The age of 2943 ± 9.3 Ma for the Canaã dos Carajás Granite is older than the 2859 ± 2 Ma (U-Pb zircon, LA-ICPMS) obtained by Feio et al. (2013), and the same is the case for the Campina Verde Tonalite, for which the presented ages are older than the 2876 ± 5.4 and 2871 ± 7.7 Ma, U-Pb SHRIMP in zircon, obtained by Moreto et al. (2015a) for the same unit. The crystallization of these rocks occurred within a 90-Ma time interval, forming the Serra dos Carajás basement during the Mesoarchean. The Rio Verde TTG (tonalite-trondhjemite-granodiorite) association and Serra Dourada Granite dated by Moreto et al. (2011) also show ages close to 2.86 Ga, denoting a slightly younger event in this region. These ages are coincident with or close in time to those obtained for the Xingu and Pium Complex (Avelar et al., 1999; Machado et al., 1991; Pidgeon et al., 2000), marking a regional event around 2.9–2.8 Ga that formed the Carajás Basin basement.

The Umuarama, Planalto, and Bom Jesus granites are part of the Neoarchean granitogenesis circa 2.75 Ga. The obtained ages imply that these granites are coeval and may be related to the extension event responsible for the Carajás Basin initiation (Trendall et al., 1998). Campina Verde Tonalite and Umuarama Granite and Pegmatite indicated lower intercept ages about 500 Ma (501 ± 150 Ma, 498 ± 35 Ma, and 474 ± 44 Ma, respectively). These ages were also observed at the Sequeirinho and Serra Dourada Granites (Moreto et al., 2015b; Moreto et al., 2011) and the Formiga Granite (Grainger et al., 2008). These Neoproterozoic ages may reflect a U-Pb disturbance caused by Araguaia Belt collision in the eastern border of the Amazonian Craton.

The Planalto Granite presents a substantial hydrothermal zircon population, indicating a 2.54-Ga event in the southern zone of the CMP. This age is in close agreement with registered hydrothermal events in the northern zone of Carajás, as the Salobo deposit (Machado et al., 1991; Tassinari et al., 2003), although it has not been identified in the southern region. This episode is likely related to the main strike-slip structural movements, such as the Carajás Fault (Pinheiro et al., 1997). It is essential to note that these shear zones and strike-slip systems record successive periods of reactivation (Holdsworth and Pinheiro, 2000; Pinheiro et al., 1997) and that extensional and contractional tectonic inheritance are known in the lithosphere (Salazar-Mora et al., 2018). These data suggest that these shallow-crustal structures operated as channels for hydrothermal fluids at various times.

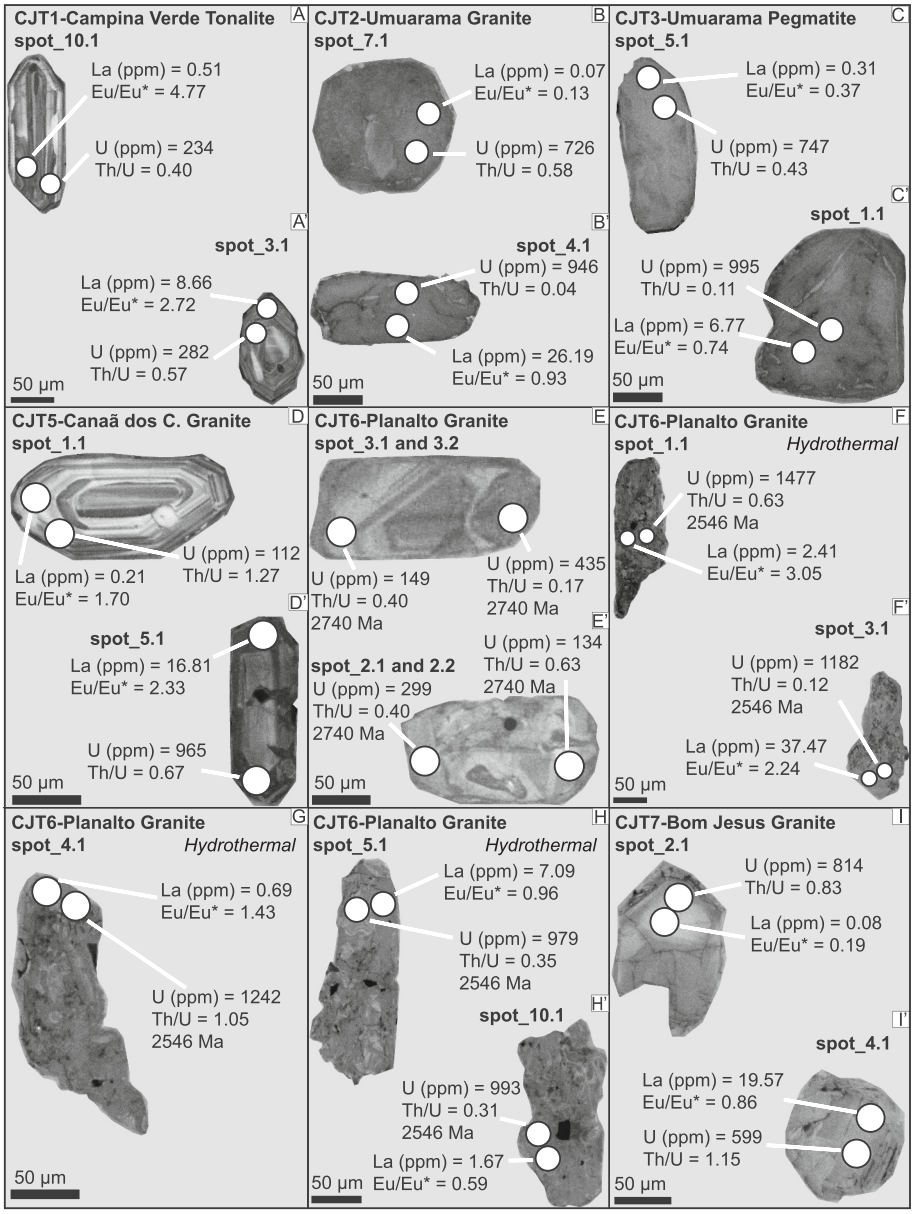

Fig. 5. SEM-Cathodoluminescence images of zircon crystals from analyzed samples from Carajás Province. (A) CJT1 – Campina Verde Tonalite has dominant magmatic zircon type (A), but some hydrothermal alteration is suggested by La enrichment and elevated Eu/Eu* (A′); (B) CJT2 – Umuarama Granite presents dominant hydrothermally altered zircon type, with elevated U contents and expressive variation of La contents (B and B′); (C) CJT3 – Umuarama Pegmatite presents the same geochemical behavior as CJT2 hydrothermally altered grains, with elevated U contents and variable La (C and C′), and both CJT2 and CJT3 present low variations on Eu/Eu*; (D) CJT5 – Canaã dos Carajás Granite is magmatic zircon, with preserved oscillatory zoning and regular U and La contents, and (D′) is a hydrothermally altered crystal, with euhedral morphology and U and La enrichment and slightly high Eu/Eu*. (E) CJT6 – Planalto Granite magmatic zircon type (E) with low U contents and preserved oscillatory zoning. A zircon grain (E′) present slight hydrothermal alteration, suggested by its massive texture. (F, G and H) CJT6 – Planalto Granite hydrothermal zircon type. These crystals present spongy texture, bread-crust texture (F, F′ and H′) diffuse rims (F, F′, G, H and H′), and anhedral morphology and are enriched in U and La and present elevated Eu/Eu*. (I) CJT7 – Bom Jesus Granite zircons are magmatic (I) with slight hydrothermal alteration (I′), suggested by elevated La contents and massive texture.

Multistage hydrothermal events must surely account for the geology of the Carajás southern zone, and continuous magmatic-hydrothermal pulses from 2.7 to 2.54 Ga are not possible. The 2.54 Ga hydrothermal record is likely linked to strike-slip fault activations and these structures' function as fluid channels. The hydrothermal event record from circa 2.5 Ga is notable throughout the province, particularly in the north, and should also be considered in mineral exploration in the southern region.

5.2. Implications of REE in zircon characterization

The zircons in the studied samples present different degrees of hydrothermal alteration, which is reflected in the REE patterns (Table 2). The magmatic zircon REE contents are those expected for igneous zircon (Hoskin and Schaltegger, 2003), and the total REE contents range from 95 to 490 ppm, while the total LREE contents range from 6 to 41 ppm. These grains also present U contents of 100 to 400 ppm and preserved oscillatory zoning, indicating that the hydrothermal alteration was not pervasive. The Eu/Eu* indicates high amplitudes ranging from 0.19 to 5.09, suggesting that the magmas were enriched in Eu, compared to Sm and Gd (Burnham and Berry, 2012; Loader et al., 2017). Another implication of elevated Eu/Eu* is titanite co-crystallization, a parameter in magmas (Loader et al., 2017), and the same effect may be observed in REE-rich hydrothermal fluids.

Hydrothermally altered zircons present massive textures, subhedral morphology, and diffuse rims, notably distinct from the magmatic type. The REE contents range from 128 to 1517 ppm and total LREE varies from 4 to 1139 ppm, indicating enrichment in these elements compared to the magmatic type. These zircons also present higher U and Th contents than the first type as well as significantly increased LREE, which is characteristic of hydrothermal alteration (Hoskin, 2005; Hoskin and Schaltegger, 2003; Takehara et al., 2018; Toscano et al., 2014; Zhong et al., 2018). Eu/Eu* values range from 0.10 to 4.35, which is indistinguishable from the magmatic type. These similar Eu/Eu* ratios may indicate that the hydrothermal fluids have comparable REE signatures to the melts that originate from the magmatic rocks. It is also possible that, during pervasive hydrothermal leaching, altered zircon geochemically re-equilibrated with the altered rocks.

The hydrothermal zircons are anhedral and massive with diffuse rims and "bread-crust" texture. These zircons have total REEs ranging from 274 to 640 ppm and LREE contents ranging from 22 to 237 ppm.

Table 2
Summary of applied zircon classification main features. Morphology and textures observed in SEM-CL images. Main geochemical features indicate the average values (σ = standard deviation) contents for selected elements and are expressed in ppm. Eu/Eu* is absolute number obtained by the expression Eu* = $(Sm_N \cdot Gd_N)^{1/2}$. $Ages_{(Ma)}$ are according to zircon type, based on classification used in this research.

Zircon type	Morphology and textures	Main geochemical features (average values)	$Ages_{(Ma)}$
Magmatic	Euhedral to subhedral; fractureless; oscillatory zoning, inherited cores (rare, but present) and microinclusions. Dominant color is light gray	Sum LREE: 21.64 (σ = 13.62); Sum REE: 204.24 (σ = 105.38); U: 229.65 (σ = 195.97); (Th + U): 389.51 (σ = 361.91); La: 0.456 (σ = 0.506); Eu/Eu*: 1.919 (σ = 1.455)	2943 ± 9.3; 2938 ± 18; 2739 ± 8.5; 2739 ± 19
Hydrothermally altered	Subhedral; massive texture (few remnant oscillatory zoning); diffuse borders. Dominant colors are gray to dark gray	Sum LREE: 162.66 (σ = 241.017); Sum REE: 565.82 (σ = 361.045); U: 529.77 (σ = 322.69); (Th + U): 803.99 (σ = 497.96); La: 25.783 (all samples) (σ = 69.667); 14.608 (except 428.0612) (σ = 19.191); Eu/Eu*: 1.710 (σ = 1.396)	2744 ± 32; 2732 ± 22
Hydrothermal	Bread-crust texture; spongy texture; diffuse borders. Dominant colors are gray, dark gray and black	Sum LREE: 72.734 (σ = 64.346); Sum REE: 379.631 (σ = 122.017); U: 1427.578 (σ = 361.463); (Th + U): 2275.654 (σ = 737.003); La: 10.964 (σ = 15.962); Eu/Eu*: 1.889 (σ = 1.123)	2546 ± 56

Hydrothermal grains are enriched in U, with contents above 900 ppm and reaching 1500 ppm. These zircons are also LREE enriched, with La contents reaching 37 ppm, which is remarkably elevated (Hoskin, 2005; Hoskin and Schaltegger, 2003; Zhong et al., 2018).

Consequently, samples CJT1 and CJT5 have predominantly magmatic zircons with some hydrothermally altered grains, while CJT2, CJT3, and CJT7 primarily contained hydrothermally altered zircon type. Sample CJT6 presents the three grain types and it was possible to distinguish the hydrothermal type and obtain the U-Pb age.

The $(Yb/Gd)_N$ and Eu/Eu* diagram (Fig. 6A) illustrates that magmatic zircons present an inverse relationship to these proposed ratios, with low $(Yb/Gd)_N$ and high Eu/Eu*. This diagram indicates that the hydrothermally altered magmatic grains are dispersed but show dominantly low $(Yb/Gd)_N$ and high variations on the Eu/Eu*. The hydrothermal type (CJT6) indicates variable $(Yb/Gd)_N$ and Eu/Eu*, although it is possible that the majority of the samples have high $(Yb/Gd)_N$ and low Eu/Eu*. In the $(Sm/Ce)_N$ versus $(Tb/Yb)_N$ diagram (Fig. 6B), the hydrothermal zircons of sample CJT6 are grouped and distinguishable from those with significant magmatic zircon populations (CJT1 and CJT5), which present higher $(Tb/Yb)_N$ and lower $(Sm/Ce)_N$ than the hydrothermal zircon, reflecting the LREE enrichment of hydrothermal zircon.

It is also noteworthy to point out that hydrothermal zircons are enriched in U, Th, and La, while hydrothermally altered zircons are LREE-enriched in most cases (Fig. 6C). The magmatic zircons generally have U contents below 500 ppm and consequently have low LREE

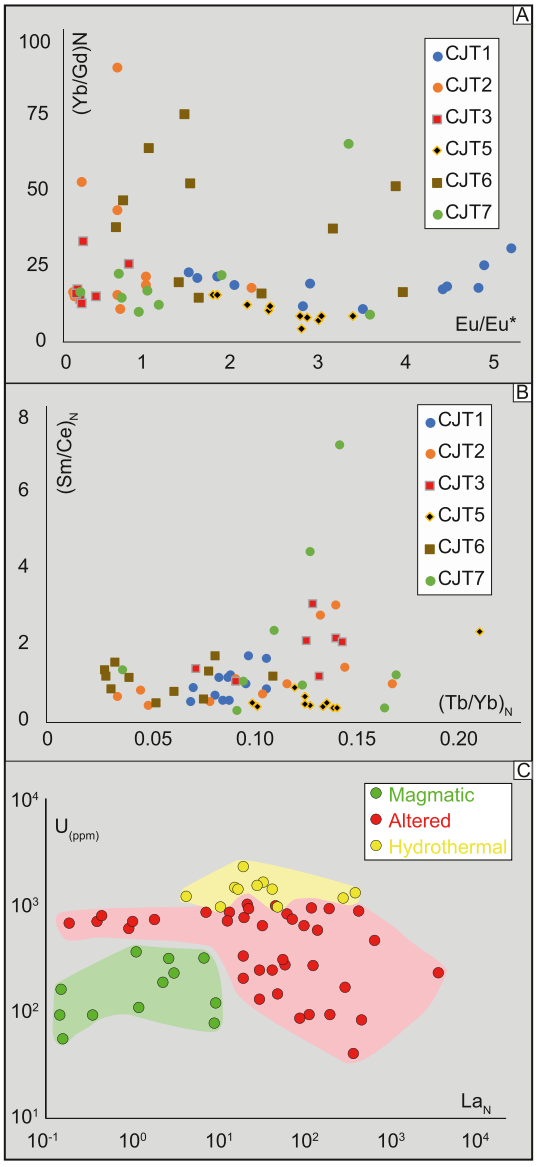

Fig. 6. REE diagrams. (A) Contrasting $(Yb/Gd)_N$ and Eu/Eu* and (B) $(Sm/Ce)_N$ versus $(Tb/Yb)_N$ diagrams for the analyzed samples. (C) $U_{(ppm)}$ and La_N diagrams for the analyzed samples with color-coded fields and symbols for magmatic, hydrothermally altered (altered for shortening) and hydrothermal zircon. (For interpretation of the references to color in this figure legend, the reader is referred to the web version of this article.)

contents (Fig. 7A).

Hydrothermal zircon differs clearly from the other two types with respect to REE content and texture. Hydrothermally altered zircons present REE-enriched contents; however, it is likely that they reflect hydrothermal disturbance rather than hydrothermal bearing. Hydrothermal zircons present U-, Th- and LREE-enriched signatures (Fig. 7A) compared to the other proposed classes of zircons. These studied zircons also present ascending enrichment in U and Th contents (Fig. 7B), grading from magmatic to hydrothermally altered to hydrothermal zircons, although the hydrothermally altered zircon types present significant variation with respect to LREE contents (Fig. 7A).

Although the analyzed rocks are barren, they are spatially related to important regional strike-slip structures and are closely related to IOCG deposits. These REE patterns in zircon suggest oxidized signatures for these hydrothermal fluids, however, for unknown reasons, no ore precipitate is immediately associated with these samples. Nevertheless,

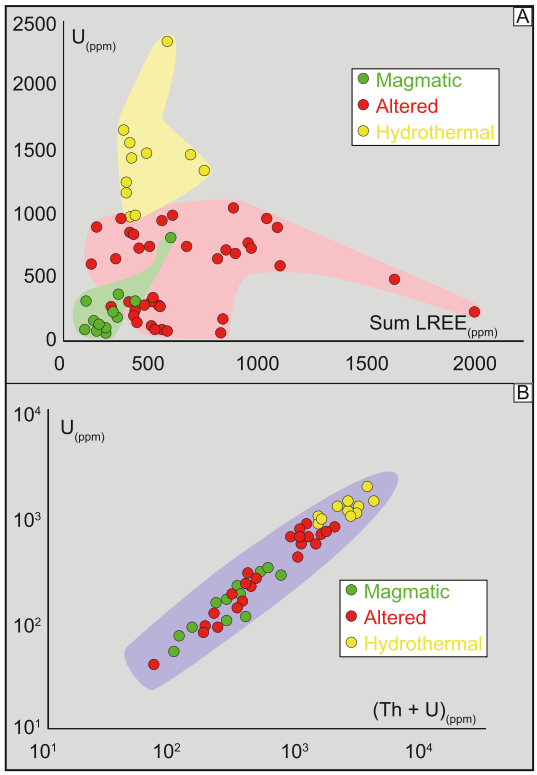

Fig. 7. (A) $U_{(ppm)}$ and Sum $LREE_{(ppm)}$ and (B) $U_{(ppm)}$ and $(Th + U)_{(ppm)}$ diagrams for the analyzed samples with color-coded fields and symbols for magmatic, hydrothermally altered (altered for shortening), and hydrothermal zircon. (For interpretation of the references to color in this figure legend, the reader is referred to the web version of this article.)

these structures presumably acted as channels, transporting fluids and ore that precipitated elsewhere around 2.54 Ga. Therefore, this age must be considered in mineral exploration in the southern region of the CMP.

6. Concluding remarks

Multistage magmatic and hydrothermal activities are indicated in the southern portion of Carajás Mineral Province based on U-Pb zircon ages and zircon REE signatures. The studied samples present three types of zircon: magmatic, hydrothermally altered magmatic, and hydrothermal, with classification based on SEM-CL images and REE and U contents. Hydrothermal zircon is distinguished by its anhedral morphology, massive and "bread-crust" texture, and diffuse rims; it is also characterized by its rich REE and U contents. The proposed classification permitted the identification of distinct grains for the same sample, and a hydrothermal event was dated separately from the magmatic at 2.54 Ga. The hydrothermal zircon age is closely related to strike-slip structures and confirms that these structures were active from the Archean age. The use of zircon classification highlights new frontiers in the study of cratonic areas aimed at tracking hydrothermal events through mineral exploration.

Supplementary data to this article can be found online at https://doi.org/10.1016/j.gexplo.2020.106679.

CRediT authorship contribution statement

Borba, M. L.: Conceptualization, methodology, data acquisition, data curation, writing- original draft preparation, and reviewing.
Tassinari, C. C. G.: supervision, writing- reviewing.
Matos, F. M. V.: Field data collection and data discussion.
Sato, K.: Methodology and data acquisition.
Huhn, S.: Field data collection and data discussion.
Ferreira, S. N.: Field data collection and data discussion.
Medeiros, C. A.: Field data collection and data discussion.

Declaration of competing interest

The authors declare that they have no known competing financial interests or personal relationships that could have appeared to influence the work reported in this paper.

Acknowledgments

The authors are grateful to the Brazilian National Council for Scientific and Technological Development for having supported part of this study (grants CNPq 438415/2017-7 and 302947/2015-9). We would like to thank the VALE Company for data access, samples, and their support for this research. The authors are also grateful to the isotope laboratory teams CPGeo-USP and GEOLAB-SHRIMP-II at the University of São Paulo for their assistance with the analytical procedures. This manuscript benefited from anonymous reviewers' suggestions that improved the quality of data presentation and discussion; the authors are grateful for the reviewers' dedication.

References

Almeida, J. de A.C., Dall'Agnol, R., Dias, S.B., Althoff, F.J., 2010. Origin of the Archean leucogranodiorite-granite suites: evidence from the Rio Maria terrane and implications for granite magmatism in the Archean. Lithos 120, 235–257. https://doi.org/10.1016/j.lithos.2010.07.026.

Almeida, J. de A.C., Dall'Agnol, R., Oliveira, M.A., Macambira, M.J.B., Pimentel, M.M., Rämö, O.T., Guimarães, F.V., Leite, A.A. da S., 2011. Zircon geochronology, geochemistry and origin of the TTG suites of the Rio Maria granite-greenstone terrane: implications for the growth of the Archean crust of the Carajás province, Brazil. Precambrian Res. 187, 201–221. https://doi.org/10.1016/j.precamres.2011.03.004.

Avelar, V.G.D.E., Lafon, J.M., Correia Jr., F.C., Macambira, M.J.B., 1999. O Magmatismo Arqueano Da Região De Tucumã-Província Mineral De Carajas: Novos Resultados Geocronológicos. Rev. Bras. Geociências 29, 453–460.

Ballard, J.R., Palin, J.M., Campbell, I.H., 2002. Relative oxidation states of magmas inferred from Ce"IV"/Ce"III" in zircon: application to porphyry copper deposits of northern Chile. Contrib. Mineral. Petrol. 144, 347–364. https://doi.org/10.1007/s00410-002-0402-5.

Bettencourt, J.S., Juliani, C., Xavier, R.P., Monteiro, L.V.S., Bastos Neto, A.C., Klein, E.L., Assis, R.R., Leite, W.B., Moreto, C.P.N., Fernandes, C.M.D., Pereira, V.P., 2015. Metallogenetic systems associated with granitoid magmatism in the Amazonian Craton: an overview of the present level of understanding and exploration significance. J. S. Am. Earth Sci. 68, 22–49. https://doi.org/10.1016/j.jsames.2015.11.014.

Borba, M.L., Matos, F., Tassinari, C.C.G., Huhn, S.R.B., Nunes, S., Medeiros, C., 2019. Rhyacian-Orosirian thermal event in the Carajás Mineral Province, Brazil. In: 2019 SEG Conference - South American Metallogeny: Sierra to Craton. Society of Economic Geologists, Santiago, Chile, pp. 8–10. https://doi.org/10.13140/RG.2.2.35425.25442.

Burnham, A.D., Berry, A.J., 2012. An experimental study of trace element partitioning between zircon and melt as a function of oxygen fugacity. Geochim. Cosmochim. Acta 95, 196–212. https://doi.org/10.1016/j.gca.2012.07.034.

Claoué-Long, J.C., King, R.W., Kerrich, R., 1990. Archaean hydrothermal zircon in the Abitibi greenstone belt: constraints on the timing of gold mineralisation. Earth Planet. Sci. Lett. 98, 109–128. https://doi.org/10.1016/0012-821X(90)90091-B.

Corfu, F., Davis, D.W., 1991. Comment on "Archean hydrothermal zircon in the Abitibi greenstone belt: constraints on the timing of gold mineralization" by J.C. Claoué-Long, R.W. King and R. Kerrich. Earth Planet. Sci. Lett. 104, 545–552. https://doi.org/10.1016/0012-821X(91)90229-B.

Dall'Agnol, R., Teixeira, N.P., Rämö, O.T., Moura, C.A.V., Macambira, M.J.B., de Oliveira, D.C., 2005. Petrogenesis of the Paleoproterozoic rapakivi A-type granites of the Archean Carajas metallogenic province, Brazil. Lithos 80, 101–129. https://doi.org/10.1016/j.lithos.2004.03.058.

DOCEGEO, 1988. Revisão litoestratigráfica da Província Mineral de Carajás Litoestratigrafia e principais depósitos minerais. In: 35th Congresso Brasileiro de Geologia: Brazil, pp. 11–54.

Feio, G.R.L., Dall'Agnol, R., 2012. Geochemistry and petrogenesis of the Mesoarchean granites from the Canaã dos Carajás area, Carajás Province, Brazil: implications for the origin of Archean granites. Lithos 154, 33–52. https://doi.org/10.1016/j.lithos.2012.06.022.

Feio, G.R.L., Dall'Agnol, R., Dantas, E.L., Macambira, M.J.B., Santos, J.O.S., Althoff, F.J., Soares, J.E.B., 2013. Archean granitoid magmatism in the Canaã dos Carajás area: implications for crustal evolution of the Carajás province, Amazonian craton, Brazil. Precambrian Res. 227, 157–185. https://doi.org/10.1016/j.precamres.2012.04.007.

Fu, B., Mernagh, T.P., Kita, N.T., Kemp, A.I.S., Valley, J.W., 2009. Distinguishing magmatic zircon from hydrothermal zircon: a case study from the Gidginbung high-sulphidation Au-Ag-(Cu) deposit, SE Australia. Chem. Geol. 259, 131–142. https://doi.org/10.1016/j.chemgeo.2008.10.035.

Grainger, C.J., Groves, D.I., Tallarico, F.H.B., Fletcher, I.R., 2008. Metallogenesis of the Carajás Mineral Province, Southern Amazon Craton, Brazil: varying styles of Archean through Paleoproterozoic to Neoproterozoic base- and precious-metal mineralisation. Ore Geol. Rev. 33, 451–489. https://doi.org/10.1016/j.oregeorev.2006.10.010.

Hanchar, J.M., Van Westrenen, W., 2007. Rare earth elemehavior in zircon – melt systems. Elements 37–42.

Hirata, W.K., Rigon, J.C., Kadekaru, K., Cordeiro, A.A.C., Meireles, E.M., 1982. Geologia regional da Província Mineral de Carajás. In: Anais I Simpósio de Geologia da Amazônia, 1. Belém, pp. 100–110.

Holdsworth, R.E., Pinheiro, R.V.L., 2000. The anatomy of shallow-crustal transpressional structures: insights from the Archaean Carajas fault zone, Amazon, Brazil. J. Struct. Geol. 22, 1105–1123. https://doi.org/10.1016/S0191-8141(00)00036-5.

Hoskin, P.W.O., 2005. Trace-element composition of hydrothermal zircon and the alteration of Hadean zircon from the Jack Hills, Australia. Geochim. Cosmochim. Acta 69, 637–648. https://doi.org/10.1016/j.gca.2004.07.006.

Hoskin, P.W.O., Schaltegger, U., 2003. The composition of zircon and igneous and metamorphic petrogenesis. Rev. Mineral. Geochem. 53, 27–62. https://doi.org/10.2113/0530027.

Lawrie, K.C., Mernagh, T.P., Ryan, C.G., Van Achterbergh, E., Black, L.P., 2007. Chemical fingerprinting of hydrothermal zircons: an example from the Gidginbung high sulphidation Au-Ag-(Cu) deposit, New South Wales, Australia. Proc. Geol. Assoc. 118, 37–46. https://doi.org/10.1016/S0016-7878(07)80045-9.

Lindenmayer, Z.G., Fleck, A., Gomes, C.H., Santos, A.B.S., Caron, R., Paula, F.C., Henrique Laux, J., Pimentel, M., Sardinha, A.S., 2005. Caracterização geológica do alvo Estrela (Cu-Au), Serra dos Carajás, pp. 137–205.

Loader, M.A., Wilkinson, J.J., Armstrong, R.N., 2017. The effect of titanite crystallisation on Eu and Ce anomalies in zircon and its implications for the assessment of porphyry Cu deposit fertility. Earth Planet. Sci. Lett. 472, 107–119. https://doi.org/10.1016/j.epsl.2017.05.010.

Ludwig, K.R., 2003. Isoplot 3.00: A Geochronological Toolkit for Microsoft Excel. Berkeley Geochronology Center Special Publication (75 p).

Ludwig, K.R., 2009. SQUID 2: A User's Manual. Berkeley Geochronology Center Special Publication (100 p).

Macambira, M.J.B., Vasquez, M.L., da Silva, D.C.C., Galarza, M.A., Barros, C.E. de M., Camelo, J. de F., 2009. Crustal growth of the central-eastern Paleoproterozoic domain, SW Amazonian craton: juvenile accretion vs. reworking. J. S. Am. Earth Sci. 27, 235–246. https://doi.org/10.1016/j.jsames.2009.02.001.

Machado, N., Lindenmayer, Z., Krogh, T.E., Lindenmayer, D., 1991. U-Pb geochronology of Archean magmatism and basement reactivation in the Carajás area, Amazon shield, Brazil. Precambrian Res. 49, 329–354. https://doi.org/10.1016/0301-9268(91)90040-H.

Marschik, R., Spangenberg, J.E., Leveille, R.A., Almeida, A.J., 2003. The Sossego iron oxide Cu-Au deposit, Carajás, Brazil. Miner. Explor. Sustain. Dev. 331–334.

Marschik, R., Mathur, R., Ruiz, J., Leveille, R.A., Almeida, A.J., 2005. Late Archean Cu-Au-Mo mineralization at Gameleira and Serra Verde, Carajás Mineral Province, Brazil: constraints from Re-Os molybdenite ages. Mineral Deposits 39, 983–991. https://doi.org/10.1007/s00126-004-0450-z.

McDonough, W.F., Sun, S.-s., 1995. The composition of the Earth. Chem. Geol. 120, 223–253. https://doi.org/10.1016/0009-2541(94)00140-4.

Monteiro, L.V.S., Xavier, R.P., Hitzman, M.W., Juliani, C., de Souza Filho, C.R., Carvalho, E. de R., 2008. Mineral chemistry of ore and hydrothermal alteration at the Sossego iron oxide-copper-gold deposit, Carajás Mineral Province, Brazil. Ore Geol. Rev. https://doi.org/10.1016/j.oregeorev.2008.01.003.

Moreto, C.P.N., Monteiro, L.V.S., Xavier, R.P., Amaral, W.S., Santos, T.J.S., Juliani, C., Filho, C.R.S., 2011. Mesoarchean (3.0 and 2.86 Ga) host rocks of the iron oxide-Cu-Au Bacaba deposit, Carajás Mineral Province: U-Pb geochronology and metallogenetic implications. Mineral Deposits 46, 789–811. https://doi.org/10.1007/s00126-011-0352-9.

Moreto, C.P.N., Monteiro, L.V.S., Xavier, R.P., Creaser, R.A., DuFrane, S.A., Melo, G.H.C., Delinardo da Silva, M.A., Tassinari, C.C.G., Sato, K., 2015a. Timing of multiple hydrothermal events in the iron oxide–copper–gold deposits of the Southern Copper Belt, Carajás Province, Brazil. Mineral Deposits 50, 517–546. https://doi.org/10.1007/s00126-014-0549-9.

Moreto, C.P.N., Monteiro, L.V.S., Xavier, R.P., Creaser, R.A., DuFrane, S.A., Tassinari, C. C.G., Sato, K., Kemp, A.I.S., Amaral, W.S., 2015b. Neoarchean and paleoproterozoic iron oxide-copper-gold events at the sossego deposit, Carajás Province, Brazil: Re-Os and U-Pb geochronological evidence. Econ. Geol. 110, 809–835. https://doi.org/10.2113/econgeo.110.3.809.

Oliveira, M.A., Dall'Agnol, R., Althoff, F.J., Leite, A.A. da S., 2009. Mesoarchean sanukitoid rocks of the Rio Maria Granite-Greenstone Terrane, Amazonian craton, Brazil. J. S. Am. Earth Sci. 27, 146–160. https://doi.org/10.1016/j.jsames.2008.07.003.

Pidgeon, R.T., Macambira, M.J.B., Lafon, J.M., 2000. Th-U-Pb isotopic systems and internal structures of complex zircons from an enderbite from the Pium Complex, Carajas Province, Brazil: evidence for the ages of granulite facies metamorphism and the protolith of the enderbite. Chem. Geol. 166, 159–171. https://doi.org/10.1016/S0009-2541(99)00190-4.

Pinheiro, R.V.L., Holdsworth, R.E., Rivalenti, G., Mazzucchelli, M., Girardi, V.A.V., Cavazzini, G., Finatti, C., Barbieri, M.A., Teixeira, W., 1997. Reactivation of Archaean strike-slip fault systems, Amazon region, Brazil. Lithos 43, 99–103. https://doi.org/10.1144/gsjgs.154.1.0099.

Pollard, P.J., Taylor, R.G., Peters, L., Matos, F., Freitas, C., Saboia, L., Huhn, S.R.B., 2018. 40Ar- 39Ar dating of Archean iron oxide Cu-Au and Paleoproterozoic granite-related Cu-Au deposits in the Carajás Mineral Province, Brazil: implications for genetic models. Mineral Deposits. https://doi.org/10.1007/s00126-018-0809-1.

Rubin, J.N., Henry, C.D., Price, J., 1989. Hydrothermal zircons and zircon overgrowths, Sierra Blanca Peaks, Texas. Am. Mineral. 74, 865–869.

Salazar-Mora, C.A., Huismans, R.S., Fossen, H., Egydio-Silva, M., 2018. The Wilson cycle and effects of tectonic structural inheritance on rifted passive margin formation. Tectonics 37, 3085–3101. https://doi.org/10.1029/2018TC004962.

Santos, J.O.S., 2003. Geotectônica dos Escudos das Guianas e Brasil-Central. In: Bizzi, L. A., Schobbenhaus, C., Vidotti, R.M., Gonçalves, J.H. (Eds.), Geologia, Tectônica e Recursos Minerais Do Barasil. Companhia de Pesquisa e Recursos Minerais, Brasília, pp. 169–226. https://doi.org/10.1641/0006-3568(2002)052[0282:tccbab]2.0.co;2.

Santos, J.O.S., Hartmann, L.A., Gaudette, H.E., Groves, D.I., McNaughton, N.J., Fletcher, I.R., 2000. A new understanding of the provinces of the Amazon Craton based on integration of field mapping and U-Pb and Sm-Nd geochronology. Gondwana Res. 3, 453–488. https://doi.org/10.1016/S1342-937X(05)70755-3.

Sardinha, A.S., Barros, C.E.M., Krymsky, R., 2006. Geology, geochemistry, and U-Pb geochronology of the Archean (2.74 Ga) Serra do Rabo granite stocks, Carajas Metallogenetic Province, northern Brazil. J. S. Am. Earth Sci. 20, 327–339. https://doi.org/10.1016/j.jsames.2005.11.001.

Sato, K., Tassinari, C.C.G., Basei, M.A.S., Siga, O., Onoe, A.T., De Souza, M.D., 2014. Sensitive High Resolution Ion Microprobe (SHRIMP IIe/MC) of the Institute of Geosciences of the University of São Paulo, Brazil: analytical method and first results. Geol. USP - Ser. Cient. 14, 3–18. https://doi.org/10.5327/Z1519-874X201400030001.

Sato, K., Tassinari, C.C.G., Basei, M.A.S., Onoe, A.T., Siga Jr., O., 2016. First REE analyses in zircon by SHRIMP at Geosciences Institute of São Paulo University: REE diffusion from apatite inclusion inside Temora zircon. In: VIII International SHRIMP Workshop. Granada, Spain, pp. 71–74.

Smythe, D.J., Brenan, J.M., 2016. Magmatic oxygen fugacity estimated using zircon-melt partitioning of cerium. Earth Planet. Sci. Lett. 453, 260–266. https://doi.org/10.1016/j.epsl.2016.08.013.

Stacey, J.S., Kramers, J.D., 1975. Approximation of terrestrial lead isotope evolution by a two-stage model. Earth Planet. Sci. Lett. 26, 207–221. https://doi.org/10.1016/0012-821X(75)90088-6.

Takehara, M., Horie, K., Hokada, T., Kiyokawa, S., 2018. New insight into disturbance of U-Pb and trace-element systems in hydrothermally altered zircon via SHRIMP analyses of zircon from the Duluth Gabbro. Chem. Geol. 484, 168–178. https://doi.org/10.1016/j.chemgeo.2018.01.028.

Tallarico, F.H.B., Mcnaughton, N.J., Groves, D.I., Fletcher, I.R., Figueiredo, B.R., Carvalho, J.B., Rego, J.L., Nunes, A.R., 2004. Geological and SHRIMP II U-Pb constraints on the age and origin of the Breves Cu-Au-(W-Bi-Sn) deposit, Carajás, Brazil. Mineral Deposits 39, 68–86. https://doi.org/10.1007/s00126-003-0383-y.

Tallarico, F.H.B., Figueiredo, B.R., Groves, D.I., Kositcin, N., McNaughton, N.J., Fletcher, I.R., Rego, J.L., 2005. Geology and SHRIMP U-Pb geochronology of the Igarapé Bahia deposit, Carajás copper-gold belt, Brazil: an Archean (2.57 Ga) example of iron-oxide Cu-Au-(U-REE) mineralization. Econ. Geol. 100, 7–28. https://doi.org/10.2113/100.1.0007.

Tassinari, C.C.G., Macambira, M.J.B., 1999. Geochronological provinces of the Amazonian Craton. Episodes 22, 174–182.

Tassinari, C.C.G., Mellito, K.M., Babinski, M., 2003. Age and origin of the Cu (Au-Mo-Ag) Salobo 3A ore deposit, Carajas Mineral Province, Amazonian Craton, northern Brazil. Episodes 26, 2–9.

Tavares, F.M., 2015. Evolução geotectônica do nordeste da Província Carajás. Tese de doutorado. UFRJ/IGEO, Rio de Janeiro (143f).

Teixeira, A.S., Ferreira Filho, C.F., Giustina, M.E.S. Della, Araújo, S.M., Silva, H.H.A.B., 2015. Geology, petrology and geochronology of the Lago Grande layered complex: evidence for a PGE-mineralized magmatic suite in the Carajás Mineral Province, Brazil. J. S. Am. Earth Sci. 64, 116–138. https://doi.org/10.1016/j.jsames.2015.09.006.

Toscano, M., Pascual, E., Nesbitt, R.W., Almodóvar, G.R., Sáez, R., Donaire, T., 2014. Geochemical discrimination of hydrothermal and igneous zircon in the Iberian Pyrite Belt, Spain. Ore Geol. Rev. 56, 301–311. https://doi.org/10.1016/j.oregeorev.2013.06.007.

Trendall, A.F., Basei, M.A.S., De Laeter, J.R., Nelson, D.R., 1998. SHRIMP zircon U-Pb constraints on the age of the Carajas formation, Grao Para Group, Amazon Craton. J. S. Am. Earth Sci. 11, 265–277. https://doi.org/10.1016/S0895-9811(98)00015-7.

VALE, 2015. Relatório Técnico: Petrografia de amostras do embasamento da Província Carajás (Monteiro, L. V.) (unpublished).

Vasquez, M., Souza, C., Carvalho, J., 2008. Mapa Geológico e de Recursos Minerais do Estado do Pará, escala 1: 1.000. 000. Programa Geologia do Brasil (PGB), Integração, Atualização e Difusão de Dados da Geologia do Brasil, Mapas Geológicos Estaduais.

Wiedenbeck, M., Hanchar, J.M., Peck, W.H., Sylvester, P., Valley, J., Whitehouse, M., Kronz, A., Morishita, Y., Nasdala, L., Fiebig, J., Franchi, I., Girard, J.P., Greenwood, R.C., Hinton, R., Kita, N.T., Mason, P.R.D., Norman, M., Ogasawara, M., Skar, O., Spicuzza, M.J., Terada, K., Tindle, A., Togashi, S., Vennemann, T., Xie, Q., Zheng, Y.F., 2004. Further characterisation of the 91500 zircon crystal. Geostand. Geoanal. Res. 28, 9–39. https://doi.org/10.1111/j.1751-908X.2004.tb01041.x.

Williams, I.S., 1998. U-Th-Pb geochronology by ion microprobe. Rev. Econ. Geol. 7, 1–35.

Xavier, R.P., Monteiro, L.V.S., Moreto, C.P.N., Pestilho, A.L.S., Melo, G.H.C., Silva, M.A. D., Aires, B., Ribeiro, C., Silva, F.H.F., 2012. The iron oxide copper-gold system of the Carajás Mineral Province, Brazil. In: Hedenquist, J.W., Harris, M., Camus, F. (Eds.), Geology and Genesis of Major Copper Deposits and Districts of the World: A Tribute to Richard H. Sillitoe. Society of Economic Geologists, p. 16. Chapter X. https://doi.org/10.5382/SP.16.1.

Zhong, S., Feng, C., Seltmann, R., Li, D., Qu, H., 2018. Can magmatic zircon be distinguished from hydrothermal zircon by trace element composition? The effect of mineral inclusions on zircon trace element composition. Lithos 314–315, 646–657. https://doi.org/10.1016/j.lithos.2018.06.029.